IEEE Access
Multidisciplinary | Rapid Review | Open Access Journal

IEEE POWER & ENERGY SOCIETY SECTION

Received 1 July 2024, accepted 19 July 2024, date of publication 7 August 2024, date of current version 19 August 2024.

Digital Object Identifier 10.1109/ACCESS.2024.3439688

RESEARCH ARTICLE

Passivity-Based Control PI for the Versatile Buck-Boost (VBB) Converter

CATALINA GONZÁLEZ-CASTAÑO[1,2], (Member, IEEE), ANTONIO VÉLIZ[3], DUBERNEY MURILLO-YARCE[4], (Member, IEEE), WALTER GIL-GONZÁLEZ[5], (Senior Member, IEEE), CARLOS RESTREPO[2,3], AND ALEJANDRO GARCÉS[5], (Senior Member, IEEE)

[1]Energy Transformation Center, Facultad de ingeniería, Universidad Andrés Bello, Santiago 7500971, Chile
[2]Principal Investigator Millennium Institute on Green Ammonia as Energy Vector (MIGA), Santiago 7820436, Chile
[3]Faculty of Engineering, Universidad de Talca, Curico 3340000, Chile
[4]Ingeniería Eléctrica, Electrónica, de Comunicaciones y Sistemas, Universidad de Oviedo, 33204 Gijón, Spain
[5]Department of Electrical Engineering, Universidad Tecnológica de Pereira, Pereira 660003, Colombia

Corresponding author: Carlos Restrepo (crestrepo@utalca.cl)

This work was supported in part by the Thematic Network "Red para la integración a gran escala de energías renovables en sistemas eléctricos (RIBIERSE-CYTED)" under Grant 723RT0150; in part by Chilean Government under Project Agencia Nacional de Investigación y Desarrollo (ANID)/FONDECYT/3220126 and Project ANID/FONDECYT/1231015; in part by the Solar Energy Research Center (SERC) Chile under Grant ANID/FONDAP/1522A0006; in part by the Millennium Institute on Green Ammonia as Energy Vector Millennium Science Initiative Program (MIGA) ANID under Grant ICN2021 023; and in part by the Project no. 6-24-9, titled Desarrollo de una metodología de control secundario para microrredes de corriente continua aisladas empleando control predictivo basado en el modelo from at Universidad Tecnológica de Pereira.

ABSTRACT Voltage and current requirements imposed by direct current loads are highly demanding in modern applications such as microgrids and electric vehicles. High-performance converters and controllers are required for these applications. The versatile buck-boost (VBB) converter has shown comparative advantages such as non-inverting output, wide bandwidth, and smooth transition between operation modes and current control loops. The control law can enhance these intrinsic advantages. In this work, a passivity-based current controller is designed and implemented for this converter. The control is based on the system's dissipative characteristic to match the desired operating point's power function. The proposed controller maintains the simplicity and robustness of a PI control while guaranteeing high performance and dynamic stability. This control does not depend on the converter's component values. Theoretical analyses are complemented with numerical simulations and experimental results on a purpose-built prototype. The proposed control shows stable and high performance in both buck and boost modes, demonstrating its effectiveness and reliability in real-world conditions, presenting for the buck and boost modes equal settling times in transitions (about to 100 μs). These benefits make it particularly suitable for demanding applications requiring robust and efficient power conversion.

INDEX TERMS Current control, noninverting buck-boost converter, passive system, PI passivity based control, PI digital control.

I. INTRODUCTION

The increasing use of renewable energies and electric vehicles have created the necessity for dc grids with high efficient conversion systems [1], [2], [3], [4], [5]. Dc-dc converters have a fundamental role in these applications to step-up (boost mode) or step-down (buck mode) dc voltages. These converters must perform both functions and supply a constant output voltage over an extensive range of input voltages [6], [7], [8], [9]. Therefore, the buck-boost family is a particularly interesting topology due to its high flexibility [10], [11], [12]. In particular, the noninverting buck-boost converter with coupled inductors and a damping network presented in the literature as the *versatile buck-boost converter* (VBB

The associate editor coordinating the review of this manuscript and approving it for publication was K. Srinivas.

converter from here on) offers advantages such as high efficiency, wide bandwidth, a soft transition between buck and boost modes [13], [14], [15], [16], [17], [18].

The possibility of controlling either input or output voltages or currents has been addressed in [13], [14], [15], and [19]. These previous works demonstrated the VBB converter may be used in modern grid applications [17]. However, the converter's performance for different control techniques (analog and digital) is of great interest to fit in the best way for all the aforementioned applications. Analog and digital techniques have been proposed in the scientific literature. Analog techniques include classic proportional-integral (PI) controls with analog implementation as presented in [13]. Besides, analog-average current control was proposed for both the input and output currents in [14]. A variation of this technique was used in [15] to improve the transitions between input and output current control loops. Digital techniques have also been studied to improve performance and straightforward implementation. The first proposed digital controller was a PI compensator for the output voltage [19]. This digital implementation improves the transition between buck and boost modes, avoiding the dead zone presented in all the noninverting buck–boost converters. Predictive control strategies have been also applied to this converter. A deadbeat control, which is a constant frequency predictive controller, was implemented with simple sampled and multi-sampled techniques in [20]. The multisampling technique minimizes the delay in tracking the control reference. In recent works, a finite control set model predictive control has been explored [21]. This control technique has a variable switching frequency, so a PI digital control with a similar equivalent frequency was also included to compare its performance.

All the previous methodologies are based on linearization, despite the nonlinear nature of the converter. A linear control might be enough for applications where the input voltage/current is approximately constant, though a wide range of operating points characterizes modern applications. This aspect is essential in renewable energy and electric vehicle applications where the operation point is constantly changing [22], [23], [24]. However, nonlinear controls are often complex and prone to instability in interconnected systems. Therefore, a control technique is required with three main characteristics: i) it must consider the nonlinear nature of the converter in order to be applied in a wide range of operation points, ii) it must be stable for interconnected applications, and iii) it must be simple to be implemented.

This paper presents a passivity-based PI control that meets the mentioned above. Passivity-based control has previously applied to classic dc-dc converters (see for example [25] and the references therein) but not for the VBB converter. Despite its attractive stability properties for interconnected systems, passivity-based control has remained in the control community. Its application has been limited in the industrial sector, where traditional approaches like PI controls are favored. Recently, the concept of passivity-based PI control has emerged. This control method integrates the robust theoretical foundations of passivity-based control with the straightforward implementation of PI controls. This approach has been applied successfully in other power applications such as the modular multilevel converter [26], the frequency control of nonlinear loads [27], [28], and the power control of energy storage systems [29], [30], [31]. However, to the best of the authors' knowledge, passivity-based PI control has not been proposed before for the VBB converter. The main contributions of this article are:

- The bilinear structure of the VBB is revealed. This structure is beneficial as it provides a more precise representation of the system dynamics. It also enables accurate adjustment of the PI controller parameters, enhances stability analysis, improves robustness against parameter variations and disturbances, and aligns well with the principles of PBC. This results in improved energy management and dissipation.
- Passivity-based PI control is proposed for the VBB converter in both boost and buck modes. This approach is advantageous because it combines the strong theoretical stability properties of passivity-based control with the simplicity and practical implementation of PI controllers. This ensures robust and efficient performance across various operating conditions.
- The performance of the proposed control is analyzed in practice through simulation and experimental results, and it is compared to digital PI control. This approach is advantageous as it offers empirical validation of the control method, showcasing its effectiveness and reliability in real-world conditions. Additionally, it highlights any enhancements or deviations in performance compared to the commonly used digital PI control.

The rest of the paper is organized as follows: in Section II, the VBB's dynamical model of coupled inductors is exposed. General concepts of passivity and the formation of the passive PI control is presented in Section III. In Section IV, PI control is designed to serve as a point of comparison for the proposed controller. Simulation and experimental results are included in Section V. Finally, the conclusions of this work are presented in Section VI.

II. BILINEAR REPRESENTATION

A schematic diagram of the converter's power circuit with *RC*-type damping network and coupled input and output inductor is shown in Figure 1. Its dynamical model is given by the following set equations:

$$\begin{aligned}
&V_0 + R_2 i_0 + L_m \frac{di_{L_m}}{dt} - u_2 v_c = 0,\\
&\quad -(i_g + i_{L_m})u_2 - \frac{v_c - v_{C_d}}{R_d} + (1-u_1) i_g = C\frac{dv_c}{dt},\\
&\frac{v_c - v_{C_d}}{R_d} = C_d \frac{dv_{C_d}}{dt},\\
&V_g - R_1 i_g - L\frac{di_g}{dt} + v_p - (1-u_1)v_c = 0,\\
&\quad -V_0 + u_2 v_c - R_2 i_0 = v_p,
\end{aligned} \tag{1}$$

where u_1 is the duty cycle of the switch Q_1 and its complementary value corresponds with the duty cycle of Q_3. While u_2 corresponds with the duty cycle of the switch Q_2 and its complementary value corresponds with the duty cycle of Q_4. In both cases $u_1, u_2 \in \{0, 1\}$. The remaining parameters are evident from Figure 1.

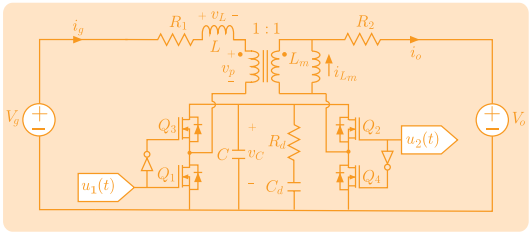

FIGURE 1. Schematic circuit diagram of the VBB converter.

By substituting $i_0 = i_g + i_{L_m}$ in (1), a new set of state equations is obtained as presented below:

$$\begin{aligned} L_m \frac{di_{L_m}}{dt} &= u_2 v_c - V_0 - R_2 i_g - R_2 i_{L_m}, \\ L \frac{di_g}{dt} &= V_g - (1 - u_1 - u_2) v_c - V_0 - (R_1 + R_2) i_g - R_2 i_{L_m}, \\ C_d \frac{dv_{C_d}}{dt} &= \frac{v_c - v_{C_d}}{R_d}, \\ C \frac{dv_c}{dt} &= \frac{v_{C_d} - v_c}{R_d} + (1 - u_1) i_g - (i_g + i_{L_m}) u_2. \end{aligned} \tag{2}$$

Thus, the VBB converter can be described by the following bilinear system

$$M\dot{x} = A_0 x + (1 - u_1) B_1 x + u_2 B_2 x + d_0, \tag{3}$$

where $x = \left[i_{L_m}, i_g, v_{C_d}, v_c\right]^T$, $d_0 = [-v_0,\ v_g - v_0,\ 0,\ 0]^\top$,

$$M = \begin{bmatrix} L_m & 0 & 0 & 0 \\ 0 & L & 0 & 0 \\ 0 & 0 & C_d & 0 \\ 0 & 0 & 0 & C \end{bmatrix},$$

$$A_0 = \begin{bmatrix} -R_2 & -R_2 & 0 & 0 \\ -R_2 & -(R_1 + R_2) & 0 & 0 \\ 0 & 0 & -\frac{1}{R_d} & \frac{1}{R_d} \\ 0 & 0 & \frac{1}{R_d} & -\frac{1}{R_d} \end{bmatrix},$$

$$B_1 = \begin{bmatrix} 0 & 0 & 0 & 0 \\ 0 & 0 & 0 & -1 \\ 0 & 0 & 0 & 0 \\ 0 & 1 & 0 & 0 \end{bmatrix}, \quad B_2 = \begin{bmatrix} 0 & 0 & 0 & 1 \\ 0 & 0 & 0 & 1 \\ 0 & 0 & 0 & 0 \\ -1 & -1 & 0 & 0 \end{bmatrix}.$$

Notice that matrix A_o is Hurwitz (*i.e.*, $A_0 + A_0^\top \prec 0$); B_1 and B_2 are skew symmetric matrices (*i.e.*, $B + B^\top = 0$), and M is a positive diagonal matrix (*i.e.*, $M \succ 0$), which contains the system components with storage capacity, such as capacitors and inductors. Notice that both B_1 and B_2 are constants. Therefore, these matrices are not affected by the circuit components or any parameter of the converter. Matrix A_0 depends on the resistance of the circuit, as given in (3).

In buck mode, we have that $u_1 = 0$ and the model is reduced as given below:

$$M\dot{x} = (A_0 + B_1)x + u_2 B_2 x + d_0,$$

whereas in boost mode, we have that $u_2 = 1$ and the model is represented as follows:

$$M\dot{x} = (A_0 + B_2)x + u_1 B_1 x + d_0.$$

Therefore, in any type of operation mode, it is possible to represent the converter as a bilinear system, namely:

$$M\dot{x} = Ax + uBx + d. \tag{4}$$

Parameters and variables of the model in each case are given in Table 1

TABLE 1. Parameters and variables of the bilinear representation of the VBB converter.

Variable or parameter	Buck mode	Boost mode
A	$A_0 + B_1$	$A_0 + B_2$
B	B_2	B_1
u	u_2	u_1
d	d_0	d_0

III. PASSIVITY-BASED PI CONTROL

A. EQUILIBRIUM POINT

The main objective is to achieve an admissible equilibrium point $\bar{x}$, as presented below:

$$0 = A\bar{x} + \bar{u}Bx + d, \tag{5}$$

for a suitable input $\bar{u}$. In this study, the control objective is to manage $\bar{x}_2 = i_{g(ref)}$. From (5), it is strait forward to find an expression for $\bar{u}$ as function of $i_{g(ref)}$, V_g, and V_0 in each operation mode. For boost operation mode, the following expression is obtained:

$$\begin{aligned} \bar{u}_1 = &\frac{V_o + 2R_2\bar{x}_2}{2R_2\bar{x}_2} \\ &\pm \frac{\sqrt{(V_o + 2R_2\bar{x}_2)^2 + 4R_2\bar{x}_2\left(V_g - V_o - \bar{x}_2(R_1 + R_2)\right)}}{2R_2\bar{x}_2}, \end{aligned} \tag{6}$$

whereas buck operation mode presents the following stationary state input:

$$\bar{u}_2 = \frac{V_o \pm \sqrt{V_o^2 + 4R_2\bar{x}_2\left(V_g - R_1\bar{x}_2\right)}}{2\left(V_g - R_1\bar{x}_2\right)}. \tag{7}$$

Note that only measures of v_g and v_0 are required to obtain control input $\bar{u}$ at the equilibrium point.

B. INCREMENTAL MODEL

The incremental model for a bilinear system is achieved by combining (3) and (5) [32], as presented below:

$$M\Delta\dot{x} = (A + uB)\Delta x + \Delta uB\bar{x}, \tag{8}$$

where Δx and Δu are defined as $\Delta x = x - \bar{x}$ and $\Delta u = u - \bar{u}$.

The incremental bilinear model (8) is passive if there exists a function $S : \mathbb{R}^n \to \mathbb{R}$ called storage function such that for all $t > 0$ and all input function u [32], the following inequality holds:

$$S(\Delta x) \leq S(\Delta x_0) + \int_0^t \Delta u^\top \Delta y dt, \tag{9}$$

where $\Delta x_0 = \Delta x(0)$.

The following energy storage function is defined:

$$S(\Delta x) = \frac{1}{2}\Delta x^\top M \Delta x, \tag{10}$$

taking the time derivative of $S(\Delta x)$, the following expression is obtained:

$$\begin{aligned}\dot{S}(\Delta x) &= \frac{1}{2}(\Delta\dot{x}^\top M\Delta x + \Delta x^\top M\Delta\dot{x}) \\ &= \frac{1}{2}\left(\Delta x^\top (A+uB)^\top + \bar{x}^\top B^\top \Delta u^\top\right) M^{-1}M\Delta x \\ &\quad + \frac{1}{2}\Delta x^\top MM^{-1}\left((A+uB)\Delta x + \Delta uB\bar{x}\right) \\ &= \frac{1}{2}\Delta x^\top (A^\top + A)\Delta x + \frac{1}{2}\Delta x^\top (uB^\top + uB)\Delta x \\ &\quad + \Delta u\Delta x^\top B\bar{x}.\end{aligned}$$

Now, taking into account that B is a skew symmetric matrix (*i.e.*, $B + B^\top = 0$) and defining an output system as

$$\Delta y = (\bar{x}^\top B^\top)\Delta x, \tag{11}$$

the time derivative of $S(\Delta x)$ can simplify as follows

$$\dot{S}(\Delta x) = \frac{1}{2}\Delta x^\top (A^\top + A)\Delta x + \Delta u^\top \Delta y, \tag{12}$$

since $A + A^\top \prec 0$, we conclude that $\dot{S}(\Delta x) \prec \Delta u^\top \Delta y$, which implies that the incremental bilinear model (8) is passive with input Δu and output Δy [30].

C. PI CONTROLLER

The bilinear system (4) can fix an admissible equilibrium point $\bar{x}$ in closed loop with a control input given by $u = \bar{u} + \Delta u$, with

$$\begin{aligned}\Delta u &= -K_p\Delta y - K_i z, \\ \dot{z} &= \Delta y,\end{aligned} \tag{13}$$

with $K_p > 0$ and $K_i > 0$. For all initial conditions of state variables x_0 and state control z_0, the passivity-based PI controller guarantees that x converges to $\bar{x}$ as time goes forward.

A bilinear system (4) in closed-loop with the passivity-based PI controller (13) is stable by defining the following the Lyapunov function candidate:

$$W(\Delta x, z) = S(\Delta x) + \frac{1}{2}\Delta z^\top K_i \Delta z. \tag{14}$$

Note that function candidate $W(\Delta x, z)$ meets the two first Lyapunov's conditions ($W(\Delta x, z) > 0\ \forall\, x \neq \bar{x} \wedge W(0,0) = 0\ \forall\, x = \bar{x}$), and its rate of shift is given by

$$\begin{aligned}\dot{W}(\Delta x, z) &= \frac{1}{2}\Delta x^\top (A^\top + A)\Delta x \\ &\quad + \Delta u^\top \Delta y + \Delta z^\top K_i \Delta\dot{z}, \\ \dot{W}(\Delta x, z) &< -\Delta y^\top K_p \Delta y < 0.\end{aligned} \tag{15}$$

Therefore, it is concluded that the closed loop control is stable.

D. CONTROL DESIGN FOR VBB CONVERTER

The state variables are defined as follows:

$$x = \left[i_{L_m}, i_g, v_{C_d}, v_c\right]^T = [x_1, x_2, x_3, x_4]^T. \tag{16}$$

The proposed control applied to the VBB converter is obtained by computing the output function Δy from (11), as presented below for the boost operation mode:

$$\begin{aligned}\Delta y_1 &= (\bar{x}^\top B_1^\top)\Delta x \\ \Delta y_1 &= x_4\bar{x}_2 - \bar{x}_4 x_2,\end{aligned} \tag{17}$$

whereas the buck operation mode admits the following output function:

$$\begin{aligned}\Delta y_2 &= (\bar{x}^\top B_2^\top)\Delta x \\ \Delta y_2 &= x_4\bar{x}_1 - \bar{x}_4 x_1 + x_4\bar{x}_2 - \bar{x}_4 x_2.\end{aligned} \tag{18}$$

To evaluate the control law in buck mode, it is necessary to know x_1 (inductor current of the magnetization branch), but this variable can not be obtained by direct measurement. However, it is known that when the VBB converter operates in continuous conduction mode away from the boundary between modes, the currents x_1 and x_2 are approximately equal. Considering this approximation, the control law in buck mode can be rewritten as

$$\Delta y_2 = x_4\bar{x}_1 + x_4\bar{x}_2 - 2\bar{x}_4 x_2. \tag{19}$$

Now, it only needs to define the uncontrolled variables to fulfill the proposed controller, which can be solved an admissible equilibrium point (5), as follows for the boost operation mode:

$$\bar{x}_4 = V_o + R_2(1 - \bar{u}_1)\bar{x}_2, \tag{20}$$

whereas the buck operation mode is presented below:

$$\bar{x}_4 = \frac{1}{\bar{u}_2}\left(V_o + \frac{R_2\bar{x}_2}{\bar{u}_2}\right), \tag{21}$$

$$\bar{x}_1 = \frac{1 - \bar{u}_2}{\bar{u}_2}\bar{x}_2. \tag{22}$$

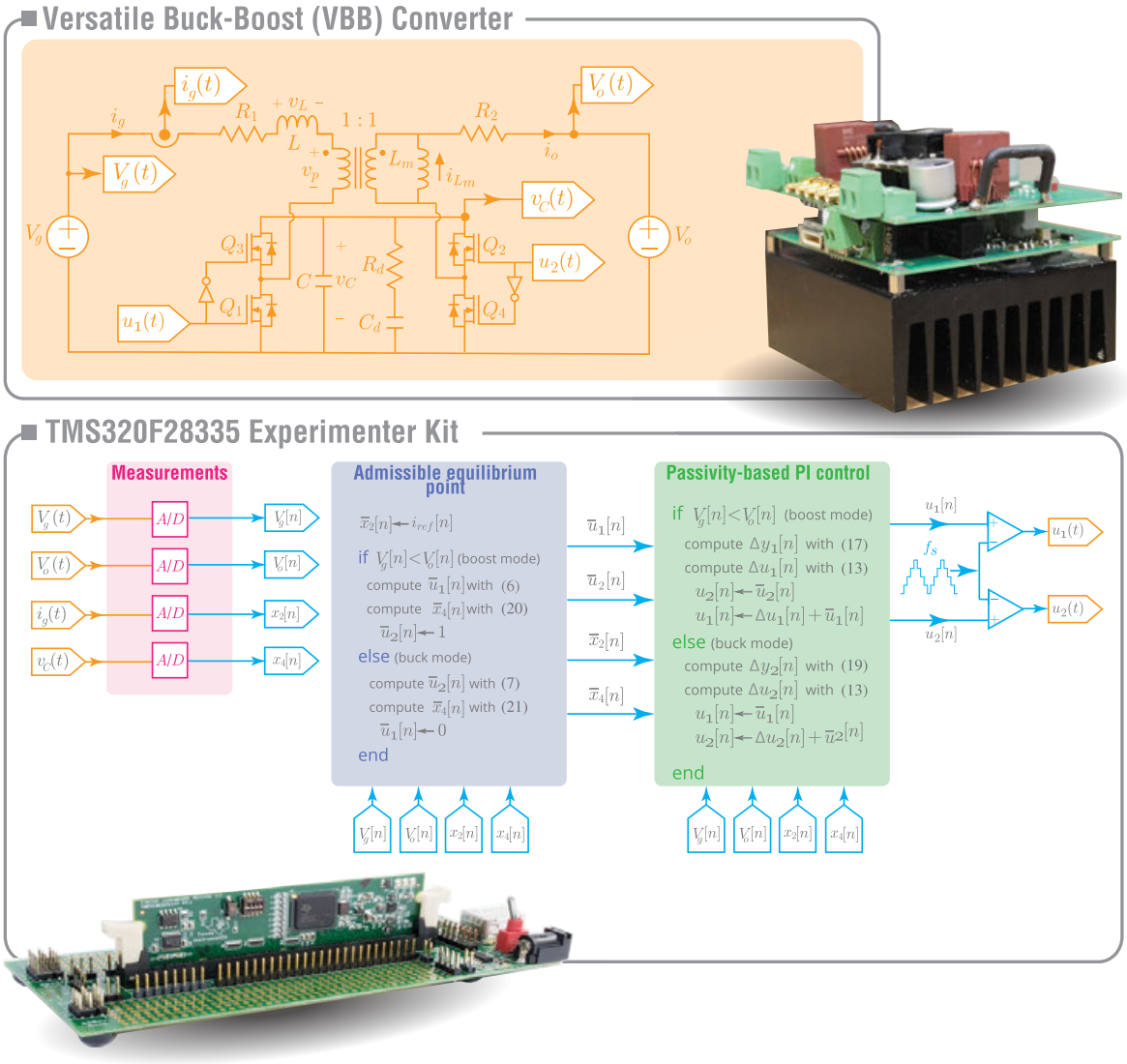

FIGURE 2. Passivity-based PI control scheme.

The passivity-based PI control scheme is illustrated in Figure 2. This figure depicts the steps to implement the digital passivity-based PI control scheme. It defines the admissible equilibrium point for each operation mode and specifies the control signals for switching. The signal controls for each operation mode are as follows:

Boost mode:

$$\begin{aligned} u_1 &= \bar{u}_1 - K_p(v_c\bar{i}_g - \bar{v}_c i_g) - K_i z_1, \\ \dot{z_1} &= v_c\bar{i}_g - \bar{v}_c i_g, \\ u_2 &= 1. \end{aligned} \tag{23}$$

Buck mode:

$$\begin{aligned} u_1 &= 0, \\ u_2 &= \bar{u}_2 - K_p(v_c\bar{i}_{Lm} + v_c\bar{i}_g - 2\bar{v}_c i_g) - K_i z_2, \\ \dot{z_2} &= v_c\bar{i}_{Lm} + v_c\bar{i}_g - 2\bar{v}_c i_g. \end{aligned} \tag{24}$$

It is important to mention that the proposed control has been performed considering the average model of the VBB converter. This means that the PI-PBC approach will work under different switching frequencies, provided that the frequency is sufficiently high to allow the use of the averaging model in the converter. In other words, the VBB converter does not enter into discontinuous mode operation.

IV. DIGITAL IMPLEMENTATION OF THE PI CONVENTIONAL CONTROL

This section presents a digital PI control that will serve to compare the proposed passive control. The PI controller is a second-order linear compensator. Initially, the compensator transfer function in continuous time is obtained using a lag network with a high-frequency pole as proposed in [33]. The design criteria used are half the switching frequency, consistent with the recommendations presented in [34]

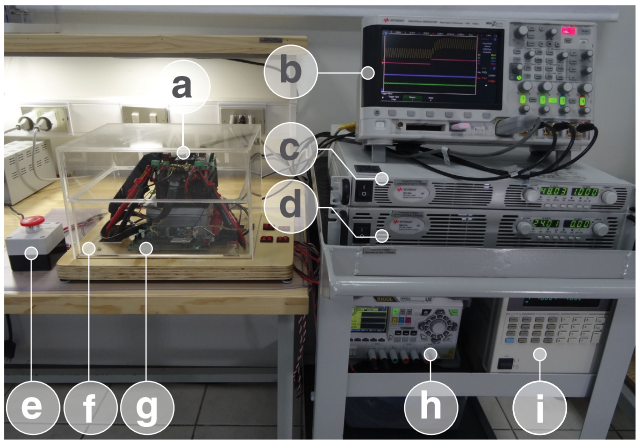

FIGURE 3. Experimental configuration for testing the proposed digital current controllers: (a) The VBB converter, (b) Oscilloscope, (c) Input dc power supply, (d) Output dc power supply, (e) Emergency stop button, (f) Acrylic case for testing circuits, (g) Digital signal controller, (h) Auxiliary power supply for DSC, converter current and voltage sensors and MOSFET Drivers, (i) Dc electronic load in constant voltage mode.

TABLE 2. Components description of the VBB converter.

Component	Description	Type
Q_1 to Q_4	Power MOSFETs	IRFB4510PBF
L	SMD Flat Wire Inductor	74435584700 Wurth Elektronik Inductance: 47 μH Dc Resistance: 19.2 $m\Omega$
C	Ceramic Capacitor X7R dielectric	CKG57NX7R2A106-M500JH 2 x 10 μF
R_d	Damping Resistor	0.5 Ω, 1 W Vishay WSL2512R5000FEA
C_d	Electrolytic Capacitor	100 μF Panasonic EEEFK2A101AM
L_m	WE-CFWI Coupled Flatwire Inductor	74485540290 Wurth Elektronik Inductance: L_1=L_2=4 x 2.9 μH Turns ratio: 1 : 1 Dc Resistance: R_1=R_2=4 x 5.6 $m\Omega$

TABLE 3. Passive PI control constants.

Constant	Buck mode	Boost mode
K_p	0.00200	0.00070
K_i	0.00044	0.00005

and [35]. On the other hand, the compensator's low-frequency pole is located at the origin to eliminate the steady-state error [36]. The zero has been located at one-tenth of the high-frequency pole. Simultaneously, the gain is adjusted through different simulations in buck and boost modes to operate with a minimum phase margin of 45^o. The second-order compensator transfer function is designed considering a switching frequency of 100 kHz.

TABLE 4. Crossover frequency (CF) and phase margin (PM) for different operation modes.

	Passive PI		Digital PI	
Operation mode	CF [kHz]	PM [deg]	CF [kHz]	PM [deg]
Buck	7.5	89.7	9.5	45.4
Boost	6.1	96.0	9.5	53.8

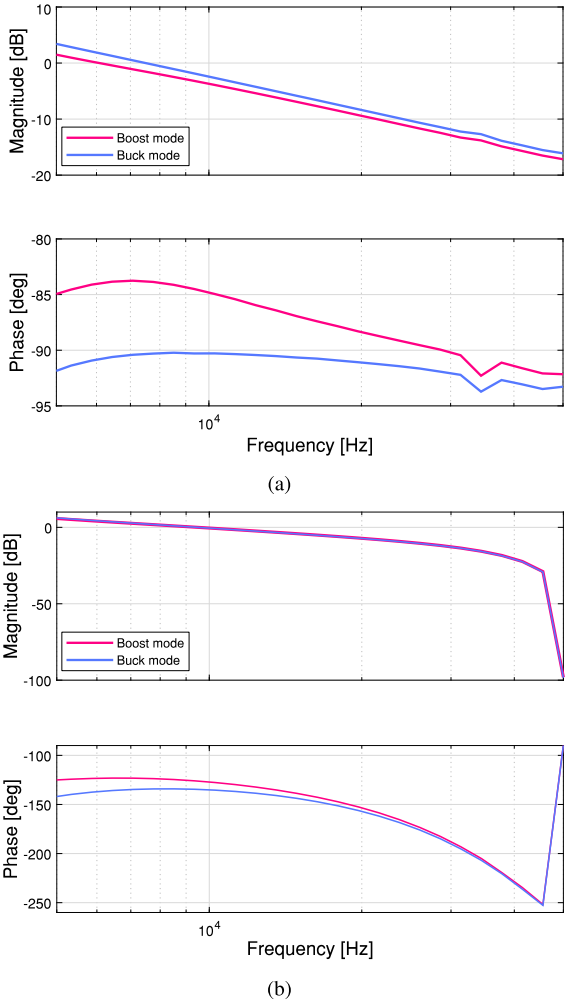

FIGURE 4. Bode plots of the input current control for the passive and digital PI controllers of the versatile buck-boost converter in boost mode (V_g = 12 V and V_o = 24 V) and buck mode (V_g = 24 V and V_o = 12 V). (a) PI passive,(b) PI digital control.

The mathematical expression for the compensator is given by (25). The parameters were selected as $K = 1800\ (sA)^{-1}$, $\tau_1 = 66\ \mu s$, $\tau_2 = 3.18\ \mu s$. Then, the Tustin transformation is applied to convert the continuous-time transfer function to discrete time, resulting in (26).

$$G(s) = K\frac{\tau_1 s + 1}{s(\tau_2 s + 1)}, \tag{25}$$

$$G(z) = \frac{0.0781z^2 + 0.011z - 0.0671}{z^2 - 0.7775z - 0.2225}. \tag{26}$$

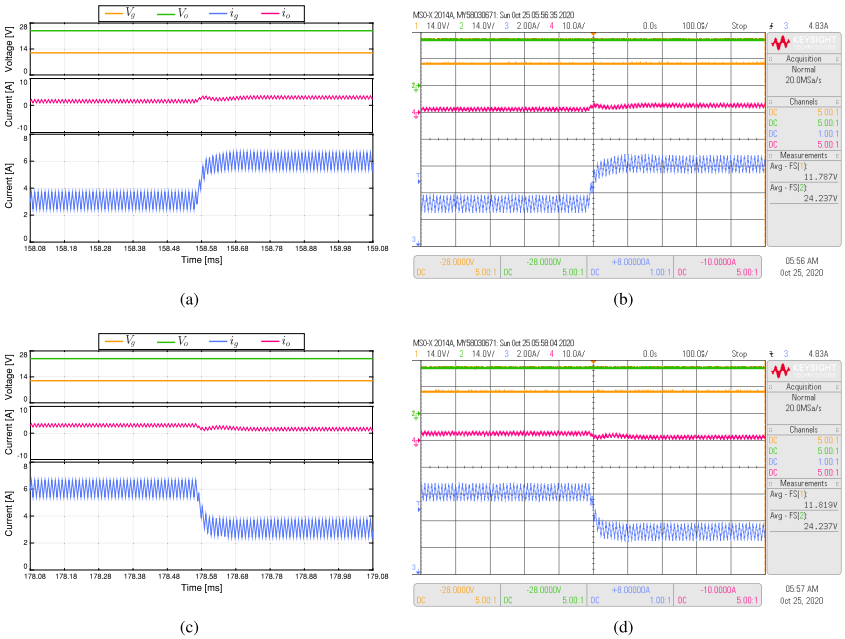

FIGURE 5. Simulated (a), (c) and experimental (b), (d) responses of the input current control based on a passivity control when the reference i_{ref} changes from: (a,b) 3 A to 6 A, and (c,d) 6 A to 3 A. The converter is operating in boost mode ($V_g = 12$ V and $V_o = 24$ V). CH1: V_g (14 V/div), CH2: V_o (14 V/div), CH3: i_g (2 A/div), CH4: i_o (10 A/div) and a time base of 100 μs.

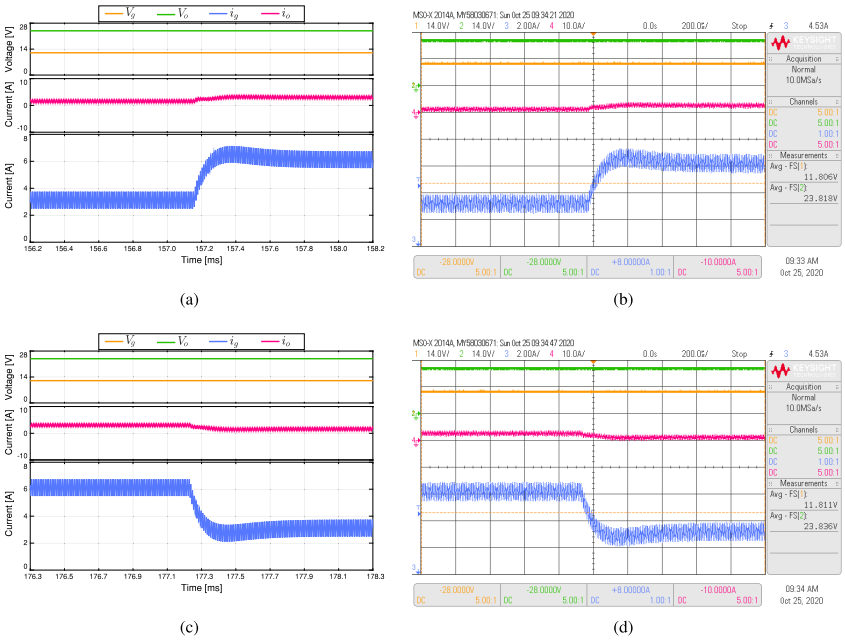

FIGURE 6. Simulated (a), (c) and experimental (b), (d) responses of the input current control based on a PI control when the reference i_{ref} changes from: (a,b) 3 A to 6 A, and (c,d) 6 A to 3 A. The converter is operating in boost mode ($V_g = 12$ V and $V_o = 24$ V). CH1: V_g (14 V/div), CH2: V_o (14 V/div), CH3: i_g (2 A/div), CH4: i_o (10 A/div) and a time base of 200 μs.

V. SIMULATION AND EXPERIMENTAL RESULTS

To validate the proposed controller's performance to regulate the converter input current, this section presents the experimental and simulated results for transient responses. The performance of this control technique is compared with the results of the classic PI controller. Results include simulation in PSIM and experimental validation in the experimental setup shown in Figure 3. The power converter parameters

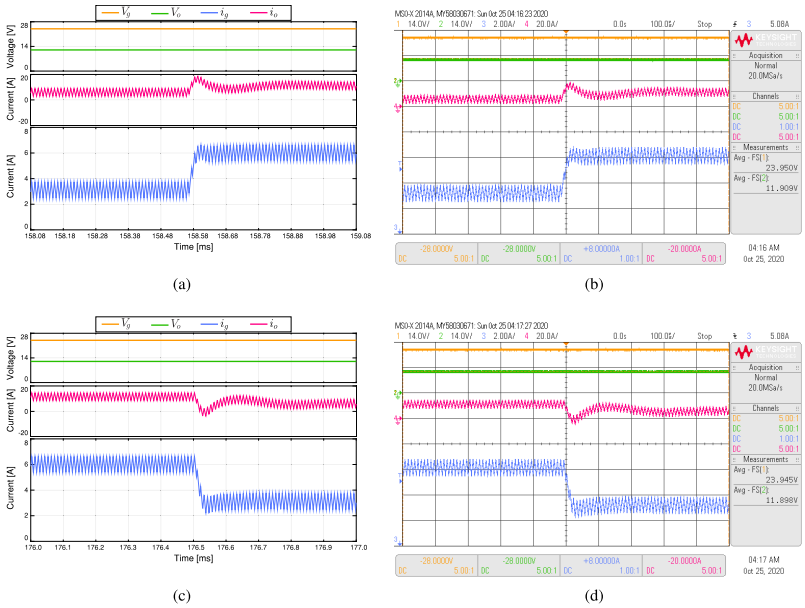

FIGURE 7. Simulated (a), (c) and experimental (b), (d) responses of the input current control based on a passivity control when the reference i_{ref} changes from: (a,b) 3 A to 6 A, and (c,d) 6 A to 3 A. The converter is operating in buck mode ($V_g = 24$ V and $V_o = 12$ V). CH1: V_g (14 V/div), CH2: V_o (14 V/div), CH3: i_g (2 A/div), CH4: i_o (20 A/div) and a time base of 100 μs.

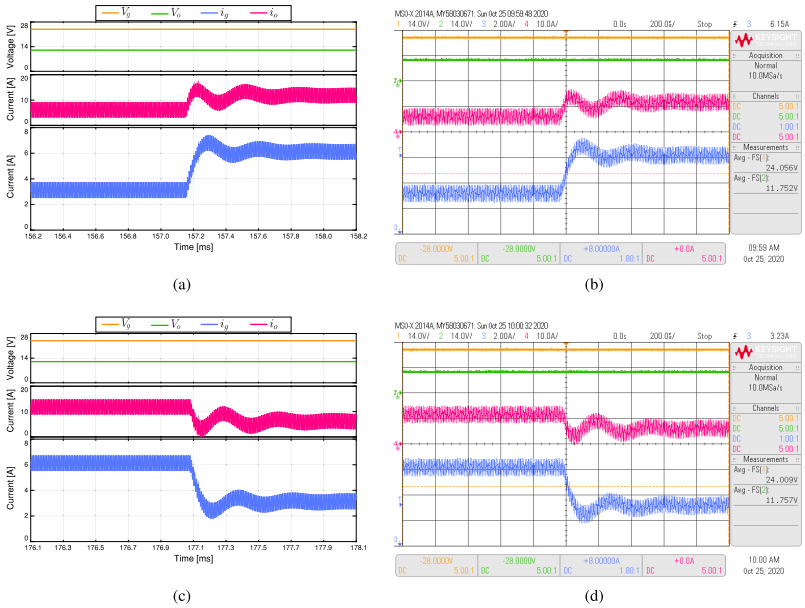

FIGURE 8. Simulated (a), (c) and experimental (b), (d) responses of the input current control based on a PI control when the reference i_{ref} changes from: (a,b) 3 A to 6 A, and (c,d) 6 A to 3 A. The converter is operating in buck mode ($V_g = 12$ V and $V_o = 24$ V). CH1: V_g (14 V/div), CH2: V_o (14 V/div), CH3: i_g (2 A/div), CH4: i_o (10 A/div) and a time base of 200 μs.

are listed in Table 2. Both controls were implemented on the TMS320F28335 Texas Instruments card at a switching frequency of 100 kHz.

Passivity-based control has proportional K_p and integral K_i gains that depend on the converter operation mode (buck and boost), which were adjusted in each case according to Table 3.

Simulated and experimental results of the passive PI control and classical PI are presented in this section. The controlled variable is the input current of the power converter. First, to evaluate the performance of both control strategies, frequency domain analysis has been conducted. Bode plots of the input-current control for the passive and

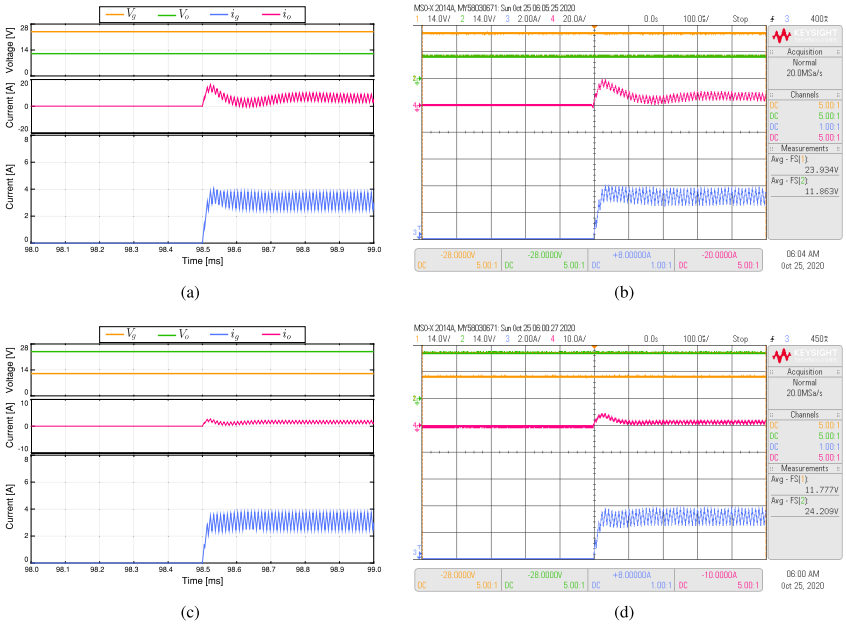

FIGURE 9. Simulated (a), (c) and experimental (b), (d) responses of converter start-up with an input current control based on a passivity control. In: (a,b) buck mode i_{ref} equal to 3 A, (c,d) boost mode i_{ref} equal to 3 A. CH1: V_g (14 V/div), CH2: V_o (14 V/div), CH3: i_g (2 A/div), CH4: i_o (20/10 A/div) and a time base of 100 μs.

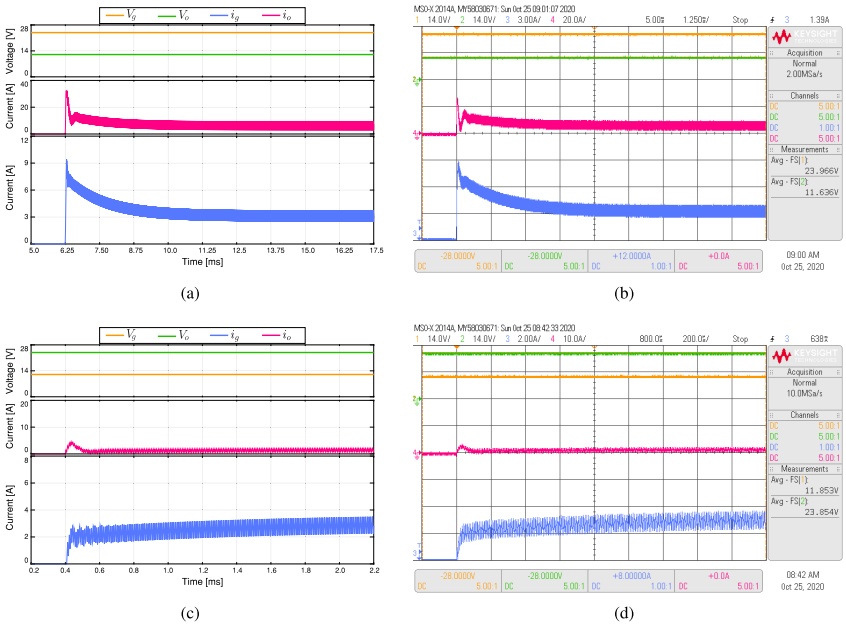

FIGURE 10. Simulated (a), (c) and experimental (b), (d) responses of converter start-up with an input current control based on a PI control. In: (a,b) buck mode i_{ref} equal to 3 A, (c,d) boost mode i_{ref} equal to 3 A. CH1: V_g (14 V/div), CH2: V_o (14 V/div), CH3: i_g (3/2 A/div), CH4: i_o (20/10 A/div) and a time base of 1.25 ms in buck mode and 200 μs in boost mode.

digital PI controllers have been generated through PSIM simulations. Figure 4 illustrates the Bode plots for the buck and boost operating modes. The crossover frequency (CF) and phase margin (PM) of the frequency responses shown in Figure 4 have been measured and are listed in Table 4 for each operating mode and current control strategy. It can be observed in Figure 4 that the passive PI offers a more significant phase margin than the digital PI, aligning with the stability concept of the proposed passive PI control.

The second part of the results section discusses time-domain responses. The results for boost mode are shown in

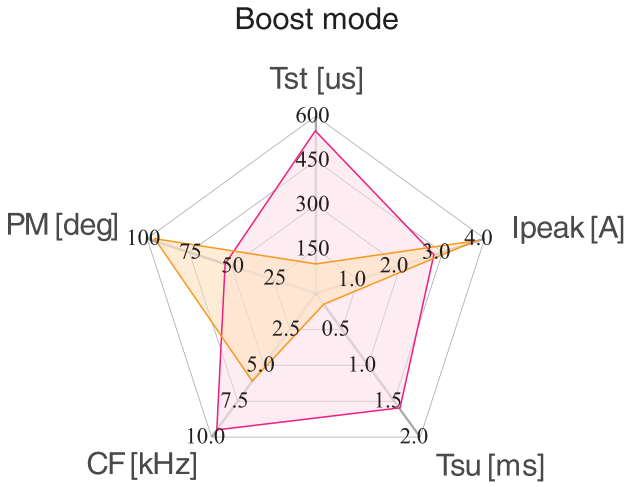

Criteria	PBC	PI
Tst [us]	100	550
Ipeak [A]	3.8	2.8
Tsu [ms]	0.15	1.6
CF [kHz]	6.1	9.5
PM [deg]	96	53.8

FIGURE 11. Comparative analysis of the results for boost mode.

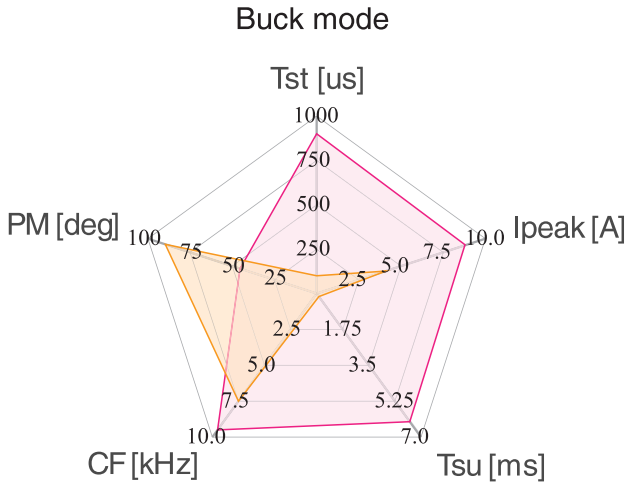

Criteria	PBC	PI
Tst [us]	100	900
Ipeak [A]	4.1	8.8
Tsu [ms]	0.15	6.25
CF [kHz]	7.5	9.5
PM [deg]	89.7	45.4

FIGURE 12. Comparative analysis of the results for buck mode.

TABLE 5. Comparison results at the start-up condition.

Mode	Boost		Buck	
Controller	PBC	PI	PBC	PI
I_{peak} [A]	3.80	2.80	4.10	8.80
T_{su} [ms]	0.15	1.6	0.15	6.25

Figures 5 and 6, while the results for buck mode are presented in Figures 7 and 8, illustrating responses to a reference change from 3 A to 6 A and from 6 A to 3 A. In all tests, the simulated results align well with the experimental results. The transitions resulting from reference changes for passive PI control are smooth, with minimal overshoot and settling times below 100 μs in both modes (see Figures 5 and 7). The response of the PI control varies based on the operation mode. In boost mode, this control exhibits similar performance to passive control with slightly higher overshoot and a settling time of (see Figure 6). (Figure 6). In buck mode, the PI control response (Figure 8) is damped oscillatory, requiring a longer time to reach (approximately (about 900 μs).

Simulation and experimental results of the start-up in both boost and buck modes are presented in Figures 9 and 10. It can be seen that the simulated and experimental waveforms are identical in all cases.

In order to realize a detailed comparison between the passivity-based control and the digital PI control in the start-up tests, the following criteria are proposed:

- I_{peak}: i_g maximum current at the start-up
- t_{su}: time elapsed from the control activation until the current i_g reaches the average value of the reference current

Table 5 summarizes the I_{peak} and t_{su} values obtained from experimental results. These values were derived from the start-up conditions depicted in Figures 9 and 10. In passive control, both buck and boost modes exhibit similar settling times (T_{su} is approximately 0.15 ms). The I_{peak} value is consistent across both modes: 3.8 A for boost mode and 4.1 A for buck mode. In PI control, the shortest settling time is observed in boost mode (T_{su} is 1.6 ms), but this value is significantly higher than the settling time in passive control. In buck mode, the highest T_{su} is achieved (6.25 ms) due to the high peak value of the i_g current at start-up. The I_{peak} is 8.8 A, which is more than four times the reference current. In boost mode, I_{peak} is 2.8 A, resulting in a shorter time to reach the reference. Figures 11 and 12 provide a summary of the results of comparison between PI-PBC and PI strategies, where T_{st} is the setting time for the results of transition seen in Figures 5, 6, 7 and 8. These results enable to conclude that passive control has a better dynamic response than the digital PI control. Furthermore, the performance indices show that the dynamic responses in buck and boost modes are equivalent (see Figures 11 and 12).

On the other hand, the PI controller has long settling times and shows varying behaviors in both buck and boost

modes. The buck mode is particularly critical because high start-up currents can lead to failures in the power converter. Although the PI controller has a wider bandwidth, the PBC controller guarantees greater stability thanks to its enhanced phase margin (compare Figures 4(a) and 4(b)).

VI. CONCLUSION

This paper presented the design and implementation of a passive PI current control for the VBB converter with coupled inductors. The proposed controller maintained the simplicity and robustness of a PI control while offering additional advantages. It ensures the stability of the VBB converter in a closed-loop system according to Lyapunov's criteria. The performance of the proposed controller was validated through simulations and experimental results both buck and boost modes, considering various operating points, reference changes, and start-up tests. Furthermore, it was compared with a digital PI controller. Frequency domain analysis revealed the proposed controller provides a larger phase margin compared to the digital PI controller. The experimental results demonstrated that the passive control exhibits superior dynamic performance, lower start-up currents, and similar behavior in both buck and boost modes.

REFERENCES

[1] F. Dastgeer, H. E. Gelani, H. M. Anees, Z. J. Paracha, and A. Kalam, "Analyses of efficiency/energy-savings of DC power distribution systems/microgrids: Past, present and future," *Int. J. Electr. Power Energy Syst.*, vol. 104, pp. 89–100, Jan. 2019.

[2] T. Capuder, D. M. Sprčić, D. Zoričić, and H. Pandžić, "Review of challenges and assessment of electric vehicles integration policy goals: Integrated risk analysis approach," *Int. J. Electr. Power Energy Syst.*, vol. 119, Jul. 2020, Art. no. 105894.

[3] M. Mishra, B. Patnaik, M. Biswal, S. Hasan, and R. C. Bansal, "A systematic review on DC-microgrid protection and grounding techniques: Issues, challenges and future perspective," *Appl. Energy*, vol. 313, May 2022, Art. no. 118810.

[4] A. Chub, N. Hassanpour, N. Yadav, T. Jalakas, A. Blinov, and D. Vinnikov, "Analysis of design requirements and optimization possibilities of partial power converter for photovoltaic string applications in DC microgrids," *IEEE Access*, vol. 12, pp. 14605–14619, 2024.

[5] R. J. Venkatesh, R. Priya, P. Hemachandu, and C. V. K. Reddy, "An optimization approach control of EV solar charging system with step-up DC–DC converter," *Anal. Integr. Circuits Signal Process.*, vol. 119, no. 2, pp. 215–232, 2024.

[6] Z. Cheng, Z. Li, S. Li, J. Gao, J. Si, H. S. Das, and W. Dong, "A novel cascaded control to improve stability and inertia of parallel buck-boost converters in DC microgrid," *Int. J. Electr. Power Energy Syst.*, vol. 119, Jul. 2020, Art. no. 105950.

[7] A. Ordono, E. Unamuno, J. A. Barrena, and J. Paniagua, "Interlinking converters and their contribution to primary regulation: A review," *Int. J. Electr. Power Energy Syst.*, vol. 111, pp. 44–57, Oct. 2019.

[8] O. D. Montoya, W. Gil-González, S. Riffo, C. Restrepo, and C. González-Castaño, "A sensorless inverse optimal control plus integral action to regulate the output voltage in a boost converter supplying an unknown DC load," *IEEE Access*, vol. 11, pp. 49833–49845, 2023.

[9] G. Chen, L. Mo, C. Jiang, and X. Qing, "From components to converters: A fundamental topology derivation method for nonresonant DC–DC converters based on graph theory," *IEEE Trans. Power Electron.*, vol. 39, no. 1, pp. 1028–1045, Jan. 2024.

[10] C. A. Ramos-Paja, D. Gonzalez Montoya, and J. D. Bastidas-Rodríguez, "Sliding-mode control of a CuK converter for voltage regulation of a DC-bus," *Sustain. Energy Technol. Assessments*, vol. 42, Dec. 2020, Art. no. 100807.

[11] M. Srinivasan and A. Kwasinski, "Control analysis of parallel DC–DC converters in a DC microgrid with constant power loads," *Int. J. Electr. Power Energy Syst.*, vol. 122, Nov. 2020, Art. no. 106207.

[12] A. Garcés-Ruiz, S. Riffo, C. González-Castaño, and C. Restrepo, "Model predictive control with stability guarantee for second-order DC/DC converters," *IEEE Trans. Ind. Electron.*, vol. 71, no. 5, pp. 5157–5165, May 2024.

[13] C. Restrepo, J. Calvente, A. Cid-Pastor, A. E. Aroudi, and R. Giral, "A noninverting buck–boost DC–DC switching converter with high efficiency and wide bandwidth," *IEEE Trans. Power Electron.*, vol. 26, no. 9, pp. 2490–2503, Sep. 2011.

[14] C. Restrepo, J. Calvente, A. Romero, E. Vidal-Idiarte, and R. Giral, "Current-mode control of a coupled-inductor buck–boost DC–DC switching converter," *IEEE Trans. Power Electron.*, vol. 27, no. 5, pp. 2536–2549, May 2012.

[15] C. Restrepo, T. Konjedic, J. Calvente, M. Milanovic, and R. Giral, "Fast transitions between current control loops of the coupled-inductor buck–boost DC–DC switching converter," *IEEE Trans. Power Electron.*, vol. 28, no. 8, pp. 3648–3652, Aug. 2013.

[16] C. González-Castaño, C. Restrepo, S. Kouro, E. Vidal-Idiarte, and J. Calvente, "A bidirectional versatile buck–boost converter driver for electric vehicle applications," *Sensors*, vol. 21, no. 17, p. 5712, Aug. 2021.

[17] C. Restrepo, C. González-Castaño, and R. Giral, "The versatile buck-boost converter as power electronics building block: Changes, techniques, and applications," *IEEE Ind. Electron. Mag.*, vol. 17, no. 1, pp. 36–45, Mar. 2023.

[18] C. González-Castaño, C. Restrepo, F. Flores-Bahamonde, and J. Rodriguez, "A composite DC–DC converter based on the versatile buck–boost topology for electric vehicle applications," *Sensors*, vol. 22, no. 14, p. 5409, Jul. 2022.

[19] C. Restrepo, T. Konjedic, J. Calvente, and R. Giral, "Hysteretic transition method for avoiding the dead-zone effect and subharmonics in a noninverting buck–boost converter," *IEEE Trans. Power Electron.*, vol. 30, no. 6, pp. 3418–3430, Jun. 2015.

[20] C. Restrepo, T. Konjedic, F. Flores-Bahamonde, E. Vidal-Idiarte, J. Calvente, and R. Giral, "Multisampled digital average current controls of the versatile buck–boost converter," *IEEE J. Emerg. Sel. Topics Power Electron.*, vol. 7, no. 2, pp. 879–890, Jun. 2019.

[21] C. Restrepo, G. Garcia, F. Flores-Bahamonde, D. Murillo-Yarce, J. I. Guzman, and M. Rivera, "Current control of the coupled-inductor buck–boost DC–DC switching converter using a model predictive control approach," *IEEE J. Emerg. Sel. Topics Power Electron.*, vol. 8, no. 4, pp. 3348–3360, Dec. 2020.

[22] X. Tang, Y. Xing, H. Wu, and J. Zhao, "An improved LLC resonant converter with reconfigurable hybrid voltage multiplier and PWM-plus-PFM hybrid control for wide output range applications," *IEEE Trans. Power Electron.*, vol. 35, no. 1, pp. 185–197, Jan. 2020.

[23] Y. Zhang, D. Zhang, J. Li, and H. Zhu, "Bidirectional LCLL resonant converter with wide output voltage range," *IEEE Trans. Power Electron.*, vol. 35, no. 11, pp. 11813–11826, Nov. 2020.

[24] L. Martínez, D. Fernández, and R. Mantz, "Passivity-based control for an isolated DC microgrid with hydrogen energy storage system," *Int. J. Hydrogen Energy*, vol. 67, pp. 1262–1269, May 2024.

[25] R. Ortega, J. A. L. Perez, P. J. Nicklasson, and H. J. Sira-Ramirez, *Passivity-based Control of Euler–Lagrange Systems: Mechanical, Electrical and Electromechanical Applications*. Berlin, Germany: Springer, 2013.

[26] R. Cisneros, R. Ortega, M. Pirro, G. Ippoliti, G. Bergna, and M. M. Cabrera, "Global tracking passivity-based PI control for power converters: An application to the boost and modular multilevel converters," in *Proc. IEEE 23rd Int. Symp. Ind. Electron. (ISIE)*, Jun. 2014, pp. 1359–1365.

[27] F. M. Serra, L. M. Fernández, O. D. Montoya, W. Gil-González, and J. C. Hernández, "Nonlinear voltage control for three-phase DC-AC converters in hybrid systems: An application of the PI-PBC method," *Electronics*, vol. 9, no. 5, p. 847, May 2020.

[28] W. He, X. Wang, M. M. Namazi, W. Zhou, and J. M. Guerrero, "A reduced-order adaptive state observer for DC–DC converters with unknown constant power load," *Control Eng. Pract.*, vol. 143, Feb. 2024, Art. no. 105785.

[29] W. Gil—González, O. D. Montoya, and A. Garces, "Direct power control of electrical energy storage systems: A passivity-based PI approach," *Electric Power Syst. Res.*, vol. 175, Oct. 2019, Art. no. 105885.

[30] W. Gil-González and O. D. Montoya, "Passivity-based PI control of a SMES system to support power in electrical grids: A bilinear approach," *J. Energy Storage*, vol. 18, pp. 459–466, Aug. 2018.
[31] S. S. Madani and A. Karimi, "Data-driven robust passivity-based controller design for grid-connected converters," *IEEE Trans. Control Syst. Technol.*, vol. 32, no. 2, pp. 300–310, Mar. 2024.
[32] R. Cisneros, M. Pirro, G. Bergna, R. Ortega, G. Ippoliti, and M. Molinas, "Global tracking passivity-based PI control of bilinear systems: Application to the interleaved boost and modular multilevel converters," *Control Eng. Pract.*, vol. 43, pp. 109–119, Oct. 2015.
[33] J. Sun and R. M. Bass, "Modeling and practical design issues for average current control," in *Proc. 14th Annu. Appl. Power Electron. Conf. Exposition. Conf.*, 1999, pp. 980–986.
[34] P. Cooke, "Modeling average current mode control [of power convertors]," in *Proc. 15th Annu. IEEE Appl. Power Electron. Conf. Expo.*, vol. 1, Feb. 2000, pp. 256–262.
[35] W. Tang, F. C. Lee, and R. B. Ridley, "Small-signal modeling of average current-mode control," *IEEE Trans. Power Electron.*, vol. 8, no. 2, pp. 112–119, Apr. 1993.
[36] *Designing With the TL5001 PWM controller*, Texas Instrum., Dallas, TX, USA, Aplication Report SLVA034A, 1995.

CATALINA GONZÁLEZ-CASTAÑO (Member, IEEE) received the degree in electronic engineering from Universidad Nacional de Colombia, Manizales, in 2008, the M.Eng. degree in electrical engineering from Universidad Tecnológica de Pereira, Colombia, in 2013, and the Ph.D. degree (Hons.) in electronic engineering, specializing in power converters for electric vehicles from Universitat Rovira i Virgili, Tarragona, Spain, in 2019. She is currently a Professor with Centro de Transformación Energética, Faculty of Engineering, Universidad Andrés Bello. She undertook the doctoral internship with the Advanced Center of Electrical and Electronic Engineering (AC3E), Valparaíso, Chile. Her main research interests include electric power quality, vehicular power systems, and the design and digital control of power converters.

ANTONIO VÉLIZ was born in Molina, Chile, in 1997. He received the bachelor's degree in civil electrical engineering from the University of Talca, Curico, Chile, in 2023. He is currently pursuing the Master of Engineering Science degree, with a mention in energy conversion. He has carried out a six-month research stay with the Power Electronics Group, TalTech, Estonia, to develop research in communications and control of dc microgrids. He is part of the Laboratory of Applications in Smart Grids (LARI in Spanish) research group headed by Prof. Carlos Restrepo. His main research interests include renewable energy and dc microgrids.

DUBERNEY MURILLO-YARCE (Member, IEEE) received the bachelor's and master's degrees in electrical engineering from Universidad Tecnológica de Pereira (UTP), Pereira, Colombia, in 2004 and 2010, respectively. From 2006 to 2018, he was a Professor with the Faculty of Engineering, Electrical and Electronic Engineering Programs, Universidad Tecnológica de Pereira. He is currently a Postdoctoral Researcher with the Power Supply Systems Group (SEA), Universidad de Oviedo. His research interests include modeling and controlling power electronic converters, renewable energies, and model predictive control.

WALTER GIL-GONZÁLEZ (Senior Member, IEEE) was born in Pereira, Colombia, in 1986. He received the B.Sc., M.Sc., and Ph.D. degrees in electrical engineering from Universidad Tecnológica de Pereira, Colombia, in 2011, 2013, and 2019, respectively, and the Ph.D. degree in renewable energy from the University of Jaén, Spain, in 2024. He previously worked as an Adjunct Professor with Institución Universitaria Pascual Bravo. He is currently a Professor with UTP. His research interests include power systems control, stability, optimization, and operation.

CARLOS RESTREPO received the bachelor's (Hons.) and master's degrees in electrical engineering from Universidad Tecnológica de Pereira, Colombia, in 2006 and 2007, respectively, and the master's and Ph.D. (Hons.) degrees in electrical engineering from Universitat Rovira i Virgili de Tarragona, Tarragona, Spain, in 2008 and 2012, respectively.

He was a Visiting Scholar with the Faculty of Electrical Engineering and Computer Science, University of Maribor, Slovenia, in 2011. From 2013 to 2014, he was a Postdoctoral Researcher with the Electrical Power Processing Group, Delft University of Technology, Delft, The Netherlands. From 2014 to 2016, he was a Professor with Departamento de Ingeniería Eléctrica, Universidad Técnica Federico Santa María, Santiago, Chile. He is currently a Professor with Departamento de Ingeniería Eléctrica, Universidad de Talca, Curico, Chile. He is the Director of the Laboratory of Applications in Smart Grids (LARI in Spanish) Research Group. His main research interests include modeling and emulator design for fuel cells, design and digital control of switched converters, and energy management of hybrid electric vehicles.

ALEJANDRO GARCÉS (Senior Member, IEEE) received the master's degree from Universidad Tecnológica de Pereira (UTP), Colombia, in 2006, and the Ph.D. degree from Norges Teknisk-Naturvitenskapelige Universitet (NTNU), Trondheim, Norway, in 2012. He is currently a Professor with the Department of Electric Power Engineering, UTP. He is a member of CIGRE and Colombian Chapter of the Society for Industrial and Applied Mathematics (SIAM). In 2020, he was awarded the Georg Forster Research Fellowship for Experienced Researchers from the Alexander von Humboldt Foundation, Germany to continue his research about optimization and control in power systems with inverter-based resources. He is an Associate Editor of IEEE TRANSACTIONS ON INDUSTRIAL ELECTRONICS and *IET Renewable Power Generation*.